



HAL
open science

A mathematical model of the circadian clock and drug pharmacology to optimize irinotecan administration timing in colorectal cancer

Janina Hesse, Julien Martinelli, Ouda Aboumanify, Annabelle Ballesta,
Angela Relógio

► To cite this version:

Janina Hesse, Julien Martinelli, Ouda Aboumanify, Annabelle Ballesta, Angela Relógio. A mathematical model of the circadian clock and drug pharmacology to optimize irinotecan administration timing in colorectal cancer. *Computational and Structural Biotechnology Journal*, 2021, 19, pp.5170-5183. 10.1016/j.csbj.2021.08.051 . hal-03539026

HAL Id: hal-03539026

<https://hal.science/hal-03539026>

Submitted on 24 Jan 2022

HAL is a multi-disciplinary open access archive for the deposit and dissemination of scientific research documents, whether they are published or not. The documents may come from teaching and research institutions in France or abroad, or from public or private research centers.

L'archive ouverte pluridisciplinaire **HAL**, est destinée au dépôt et à la diffusion de documents scientifiques de niveau recherche, publiés ou non, émanant des établissements d'enseignement et de recherche français ou étrangers, des laboratoires publics ou privés.



Distributed under a Creative Commons Attribution - NonCommercial - NoDerivatives 4.0 International License

1 A mathematical model of the circadian clock and drug pharmacology to optimize
2 irinotecan administration timing in colorectal cancer

3

4 **Janina Hesse**^{1,2,†}, **Julien Martinelli**^{3,4,5,†}, **Ouda Aboumanify**^{2,6,†}, **Annabelle Ballesta**^{2,3*}, **Angela**
5 **Relógio**^{1,2,6*}

6 ¹Institute for Systems Medicine, Department of Human Medicine, MSH Medical School Hamburg –
7 University of Applied Sciences and Medical University, Hamburg 20457, Germany

8 ²Institute for Theoretical Biology (ITB), Charité - Universitätsmedizin Berlin, corporate member of Freie
9 Universität Berlin, Humboldt - Universität zu Berlin, and Berlin Institute of Health, Berlin 10117,
10 Germany³INSERM U900, Saint-Cloud, France; Institut Curie, Saint Cloud, France; Paris Saclay
11 University, France; MINES ParisTech, CBIO - Centre for Computational Biology, PSL Research
12 University, Paris, France

13 ⁴UPR 'Chronotherapy, Cancers and Transplantation', Faculty of Medicine, Paris Saclay University,
14 Campus CNRS, 7 rue Guy Moquet, 94800 Villejuif, France.

15 ⁵Lifeware Group, Inria Saclay Ile-de-France, Palaiseau, 91120, France

16 ⁶Molecular Cancer Research Center (MKFZ), Medical Department of Hematology, Oncology, and
17 Tumor Immunology, Charité - Universitätsmedizin Berlin, corporate member of Freie Universität Berlin

18

19 † These authors contributed equally to this work

20 * Correspondence: annabelle.ballesta@inserm.fr and angela.relogio@charite.de,
21 angela.relogio@medicalschooll-hamburg.de

22

23

24

25

26

27 Competing Interests: The authors declare no competing interests.

28 **Abstract**

29 Scheduling anticancer drug administration over 24h may critically impact treatment success in a patient-
30 specific manner. Here, we address personalization of treatment timing using a novel mathematical model
31 of irinotecan cellular pharmacokinetics and –dynamics linked to a representation of the core clock and
32 predict treatment toxicity in a colorectal cancer (CRC) cellular model. The mathematical model is fitted
33 to three different scenarios, mouse liver, where the drug metabolism mainly occurs, and two human
34 colorectal cancer cell lines representing an *in vitro* experimental system for human colorectal cancer
35 progression. Our model successfully recapitulates quantitative circadian datasets of mRNA and protein
36 expression together with timing-dependent irinotecan cytotoxicity data. The model also discriminates
37 time-dependent toxicity between the different cells, suggesting that treatment can be optimized in a time-
38 dependent manner according to the cellular clock. Our results suggest that the time-dependent
39 degradation of the protein mediating irinotecan activation, as well as an oscillation in the death rate play
40 an important role in the timing of drug toxicity. In the future, this model can be used to support
41 personalized treatment scheduling by predicting drug toxicity based on the patient’s gene expression
42 profile.

43

44

45

46

47

48

49 **Keywords:** chronotherapy, irinotecan pharmacodynamics, translational-transcriptional networks,
50 circadian rhythms, molecular circadian profiles, colorectal cancer

51

52

53 **1. Introduction**

54 Mammalian physiological and behavioural processes follow a daily rhythm of approximately 24 h, which
55 is regulated by the circadian system. In mammals, the suprachiasmatic nuclei (SCN), a central pacemaker
56 located in the brain, accounts for organismal entrainment to the geophysical time, primarily via light
57 cues. The SCN passes on time information, in the form of physiological signals, to peripheral clocks,
58 located in each nucleated cell of the organism. The cellular circadian clock is a molecular machinery of
59 interconnected transcriptional-translational feedback loops that produces sustained 24h-oscillations [1].
60 Via the regulation of clock-controlled genes (CCGs), the circadian clock controls the timing of multiple
61 cellular and organismal processes, including the cell division cycle, DNA repair or energy metabolism
62 and the immune system [2-4]. Large inter-individual differences have been observed in several endpoints
63 aiming to measure circadian rhythms, from chronotype questionnaires to melatonin onset timing or
64 circadian biomarkers measured by wearables [5]. Sex appears as a major determinant of circadian
65 rhythms, as women, in general, have higher amplitude behavioural rhythms than men [6]. The disruption
66 of circadian rhythms leads to mis-regulation in the timing of cellular processes and organ functions, and
67 accumulating evidence points to a negative impact on human health. Again, sex differences exist, as
68 women tend to be more resilient to circadian disruption as compared to men [6]. Several pathologies
69 have been associated to the mis-regulation of the circadian system including cardiovascular diseases,
70 metabolism disorders and cancer [7, 8].

71 Also, most physiological processes involved in the transport and metabolism of xenobiotics are regulated
72 in a time-dependent manner, which impacts the pharmacokinetics (PK) of numerous drugs that may vary
73 largely depending on the administration timing [9, 10]. On the other hand, several drugs target circadian
74 regulated genes. Recent findings showed that more than 50% of the top 100 best-selling drugs in the
75 United States target products of circadian genes [11]. Thus, timing drug administration may also impact
76 drug pharmacodynamics (PD) and eventually treatment outcome. In the field of cancer management,
77 several clinical studies have addressed the effect of timing medications for treatment optimization –
78 chronotherapy – with promising results [8, 12-14]. Giacchetti and colleagues reported data from three
79 international Phase III clinical trials involving 842 patients (345 females and 497 males) treated with 5-
80 fluorouracil, leucovorin and oxaliplatin administered as chronomodulated or conventional infusions [15].
81 The results showed that male patients lived significantly longer on chronomodulated chemotherapy
82 compared to conventional chemotherapy. Yet, while this specific chronomodulated administration
83 scheme showed a beneficial trend in males, leading to an increase in overall survival (OS), an increase
84 in OS was reported in females undergoing this chronomodulated regimen, in comparison to a control
85 group receiving the conventional therapy [15]. Moreover, a recent international clinical trial concluded
86 that irinotecan hematological and clinical toxicities were lower for morning administration in men and
87 for early afternoon infusion in women, based on colorectal cancer patients receiving the drug in
88 combination with 5-fluorouracil and oxaliplatin [16]. Such results highlight the need for more research
89 in this field to understand inter-patient discrepancies and enable safe and efficient clinical application of
90 chronotherapy. Given the reported alterations in circadian gene expression profiles of cancer cells [17],
91 administering anticancer treatment at a time of least toxicity to healthy tissues is likely to provide a higher
92 selectivity relative to the toxic effect of chemotherapy on healthy cells. In addition, by timing treatment,
93 it would be possible to increase the tolerated dose, or prevent treatment discontinuation, to achieve a
94 more effective toxicity to the tumor cells [8].

95 Chronotherapy might be more efficient when adapted to the internal time of the patient. Yet, the
96 definition of a single internal time is challenging since the circadian timing system involves multiple
97 inter-connected central and peripheral oscillating processes [18]. We suggest to base chronotherapy
98 individualization on the patient's circadian profiles of selected genes including core-clock genes and
99 genes involved in drug pharmacology. Several patient-friendly methods for measuring clock gene

100 expression using saliva or blood sampling have been recently tested in the clinics [18]. Such patient
101 datasets, combined with mathematical modeling and machine learning may allow to predict the times of
102 least toxicity to healthy tissues, and optimal antitumor efficacy for a particular patient [18]. In particular,
103 computational models representing the chronopharmacology of a specific drug can help to predict
104 therapy time windows of decreased toxicity and optimal efficacy [18]. Such models can also be optimized
105 for a given patient and used to generate personalized treatment timing indications. In the past years,
106 several ODE (ordinary differential equation) models have been developed, which either aim to model
107 the circadian clock network [19-24] or the biochemical and biophysical interplay between the circadian
108 timing system and a given drug [25-27]. These chronoPK-PD models consider both the impact that the
109 organism has on the drug, i.e. its PK, as well as the impact of the drug on the organism, i.e. its PD, and
110 further include the control of the circadian time system on these processes.

111 Currently, there is a gap between existing mathematical models for the core-clock network and
112 mathematical models of drug PK-PD. Here we aimed at merging the core-clock network with a model
113 of the chronoPK-PD of irinotecan, an anticancer drug widely used against digestive malignancies. We
114 generated a new mathematical model, which enables predictions of the cytotoxicity timing for irinotecan,
115 having as an input the circadian gene expression of a set of core clock and irinotecan metabolism-related
116 mRNAs. For that, we refined and combined two previously published ODE mathematical models, a core
117 clock from Relógio *et al.* [23] and a model of irinotecan chronoPK-PD from Ballesta *et al.* [26, 27],
118 which have been successfully used for simulating the mammalian core clock and the time-dependent
119 cytotoxicity of irinotecan, respectively. The core-clock model was refined using newly available
120 quantitative circadian datasets of gene and protein expression in the liver of C57Bl6 male mice.
121 Representing the clock of the liver is important in view of predicting the drug metabolism that mainly
122 occurs in that organ in the whole-body scenario [28, 29]. To connect it with the PK-PD model, we
123 extended the transcription-translation network of the core clock with a set of irinotecan-related genes.
124 We fitted our new clock-irinotecan model with transcriptomic data from an *in vitro* colorectal cancer
125 (CRC) experimental progression model and carried out time-dependent irinotecan treatment in both cell
126 lines across 24h. The CRC *in vitro* progression model includes two cell lines derived from the primary
127 tumor (SW480), and from a metastasis site (SW620), of the same patient, which are known to display
128 different circadian profiles [30].

129 Our mathematical model for timing of irinotecan cytotoxicity nicely reproduced gene circadian
130 expression as well as experimental data obtained via constant monitoring of cytotoxicity for both cell
131 lines. In addition, we found that particular parameters associated with *BMAL1* and *CLOCK* (*BMAL1*
132 degradation rate, *CLOCK* activation rate, cytosolic *BMAL1* degradation rate), show high sensitivity,
133 high impact on drug toxicity emphasizing the relevance of the core clock for irinotecan PK-PD, and
134 propose candidates for molecular biomarkers of drug chronotherapy (e.g. CES and UGT1A1).

135

136

137 2. Material and Methods

138

139 2.1. Cell culture

140 SW480 (ATCC® CCL-228™), SW620 (ATCC® CCL-227™) cell lines were maintained in Dulbecco's
141 Modified Eagle Medium (DMEM) low glucose (Lonza, Basel, CH) culture medium supplemented with
142 10% fetal bovine serum (FBS) (Life technologies, Carlsbad, CA, USA), 1% penicillin-streptomycin (Life
143 technologies), 2 mM Ultraglutamine (Lonza) and 1% HEPES (Life technologies). Cells were incubated
144 at 37 °C in a humidified atmosphere with 5% CO₂. The SW480 cell line originated from a surgical
145 specimen of a primary tumour of a moderately differentiated colon adenocarcinoma (Dukes' type B) of
146 a 51-year-old Caucasian male (blood group A, Rh+). The SW620 cell line was derived from a lymph
147 node metastasis (Dukes' type C) taken from the same patient one year later.

148 2.2. shRNA-mediated knockdown

149 For the knockdown of *BMAL1*, a TRC lentiviral shRNA glycerol set (Dharmacon, Lafayette, CO, USA)
150 specific for *BMAL1* was used consisting of five individual shRNAs. The construct that gave best
151 knockdown efficiency was determined by gene expression analysis and used for further experiments.

152 2.3 RNA extraction

153 Total RNA isolation was performed using the RNeasy Mini kit (Qiagen, Venlo, NL) according to the
154 supplier's manual. Medium was discarded and cells were washed twice with PBS and lysed in RLT buffer
155 (Qiagen) prior to the purification procedure. RNA was eluted in 30 µl RNase-free water. Final RNA
156 concentration measurement was performed using a Nanodrop 1000 (Thermo Fisher Scientific).

157 2.4 c-DNA and synthesis RT-qPCR

158 For Real Time quantitative PCR (RT-qPCR) analysis, the extracted RNA was reverse transcribed into
159 cDNA (4ng/µl) using random hexamers (Eurofins MWG Operon, Huntsville, AL, USA) and Reverse
160 Transcriptase (Life technologies). RT-qPCR was performed using SsoAdvanced Universal SYBR Green
161 Supermix (Bio-Rad Laboratories, Hercules, CA, USA) in 96-well plates. *GAPDH* human QuantiTect
162 Primer assays (Qiagen) was used as reference housekeeping gene due to its high abundance and to the
163 lack of circadian oscillations, as confirmed by a cosinor analysis carried out in microarray and RNA-Seq
164 data for SW480 cells (**Supplementary Figure 2d**). Primers:

| Primer | Sequence (5'->3') |
|---------------|----------------------|
| PER2 forward | AGCCAAGTGAACGAACTGCC |
| PER2 reverse | GTTTGACCCGCTTGGACTTC |
| NR1D1 forward | CTCCATCGTCCGCATCAATC |
| NR1D1 reverse | AACGCACAGCGTCTCG |
| ARNTL forward | AACCTTCCCACAGCTCACAG |

| | |
|---------------|-----------------------|
| ARNTL reverse | CTCTTTGGGCCACCTTCTCC |
| TOP1 forward | CCAAGCATAGCAACAGTGAAC |
| TOP1 reverse | GAGGCTCGAACCTTTTCCTC |

165 **Table 1:** Primers used for the RT-qPCR analysis of SW480 and SW620 cell lines. The primers for mouse
166 can be found in the original publication [31], in the Supplementary File S2.
167

168 The qPCR reaction was performed using a CFX Connect Real-Time PCR Detection System
169 (Biorad). Relative gene expression was calculated using the $2^{-\Delta\Delta C_t}$ method [32]. Biological and technical
170 replicates were included into the analysis.

171 2.5 Time-dependent treatment with irinotecan

172 SW480 and SW620 cells were seeded in 96-well plates at 5000 cells and total volume 150 μ L per well.
173 The cells were synchronized by medium change at 4 different time points (6 h, 12 h, 18 h and 24 h)
174 before treatment with 2 μ M of irinotecan. Cells (at 60% confluence at the start of measurements) were
175 incubated at 37 $^{\circ}$ C in a humidified atmosphere with 5% CO₂. The corresponding untreated control
176 condition was measured in parallel with the treated cells. Cytotoxicity was evaluated in real time with
177 the IncuCyte[®] S3 Live-Cell system. Cytotox dyes are inert, non-fluorescent and do not enter viable cells,
178 when added to the cell culture. In dying cells, the membrane integrity is lost, the cytotox dye enters the
179 cells and fluorescently labels the nuclei. The cells are then identified and quantified by the appearance
180 of red labelled nuclei. Because confluency saturated after 84.5 h for the control conditions, the analysis
181 was restricted to 84.5 h, compare with **Supplementary Fig. 7**.

182
183

184 2.6 Omics data

185 The models were fitted to microarray time series data of 24 hours sampled with an interval of 3 hours for
186 the SW480 and SW620 cells and of 48 hours sampled with an interval of 2 hours for the liver, which was
187 scaled to concentrations based on RNA-seq data. The microarray data and RNA-seq data for liver tissue
188 was published by Zhang *et al.* 2014, accession numbers GSE54650 and GSE54652 [11]. For the SW480
189 and SW620 cells, the microarray time series data was published by El-Athman *et al.* 2018, accession
190 number E-MTAB-5876 [33], and the RNA-seq time series data was published by El-Athman *et al.* 2019,
191 accession number E-MTAB-7779 [34]. To relate the microarray data with concentrations, the following
192 steps were done for each gene separately. RNA-seq transcript data was used to calculate the temporal
193 mean of the expression in TPM, which was then converted into mean concentrations in mol/L by a simple
194 rescaling, see **Supplementary Information** for details. The microarray data was first unlogged (2^{values})
195 as the data was given in fold change. Then the data was rescaled such that its mean expression matched
196 that of the RNA-seq derived mean concentration, i.e. for a time series x of the original microarray data,
197 we used $C * 2^{x/\langle x \rangle}$, where $\langle \cdot \rangle$ denotes a temporal mean, and C is the concentration calculated for this
198 gene based on the RNA-seq data. For gene families, genes with good oscillations were selected as
199 representative gene for the gene family, as denoted in the figures.

| Dataset | Organ / Cell line | Used for model | Acquisition technique | Accession number |
|--|--|---|---|---|
| Narumi <i>et al.</i> 2016 | Mouse liver (WT mouse and Bmal1-/-) | Liver core-clock | mRNA: RT-qPCR proteins: mass spectrometry | RNA-seq: GSE54652 Microarray: GSE54650 |
| Zhang <i>et al.</i> 2014 | Mouse liver | Liver transcription-translation network | mRNA: microarray and RNA-seq | GSE54650 and GSE54652 |
| Wang 2017 | Mouse liver | Liver core-clock | Nuclear proteins: mass spectrometry | E-MTAB-5876 |
| El-Athman <i>et al.</i> 2018 | SW480 / SW620 | CRC core-clock CRC full model | mRNA: microarray | E-MTAB-7779 |
| El-Athman <i>et al.</i> 2019 | SW480 / SW620 | CRC core-clock CRC full model | mRNA: RNA-seq | E-MTAB-7779 |
| Hesse <i>et al.</i> 2021 | SW480 / SW620, control and siRNA Bmal1 | CRC core-clock CRC full model | mRNA: RT-qPCR | NA |
| Dulong <i>et al.</i> 2015; Ballesta <i>et al.</i> 2011 | Caco-2 human colorectal cancer cell line | CRC full model | CPT11 and SN38 cellular PK: HPLC TOP1 activity: DotBlot CPT11 and SN38 cytotoxicity: viability assays | NA |
| Hesse <i>et al.</i> 2021 | SW480 / SW620 | CRC full model | CPT11 cytotoxicity | NA |
| Zheng <i>et al.</i> 2019 | Mouse liver | Liver core-clock | Cytoplasmic and nuclear proteins CLOCK and BMAL abundance: immunoprecipitation | NA |
| Aryal <i>et al.</i> 2017 | Mouse liver | Liver core-clock | Cytoplasmic proteins PER and CRY: immunodepletion | NA |
| Schwanhäusser <i>et al.</i> 2011 | Mouse fibroblasts NIH3T3 | Liver core-clock | mRNA transcription rates: RNA-seq | SRA030871 |

200 Table 2: Resources for the data used in the current study.

201

202 2.7 Mathematical model

203 Model equations and parameters of the core clock are listed in the **Supplementary Information,**
204 **Supplementary Equations (1.1-18)** and **Table 2**, model equations and parameters of the clock-
205 irinotecan model are listed in **Supplementary Equations (3.1-30)** and **Table 6**. Parameter optimization
206 was done using the evolutionary algorithm CMA-ES [35]. The cytoplasm/nucleus volume ratio was set
207 for CRC cells to 5 (manual curation). Computations for the core clock were carried out on a laptop with
208 i5 2.9 GHz dual core processor using Python's pycma for the optimization and Python's

209 scipy.integrate.odeint for the numerical integration (method: lsoda, relative tolerance = absolute
210 tolerance = 10^{-12} . Computations for the clock-irinotecan network were carried out on a compute cluster
211 with the same Python packages. Model fits are restricted to oscillating mRNAs, with a minimum relative
212 amplitude of 5%, i.e. $(\max - \min) / \max > 0.05$ for each gene expression time series. The fit of the clock-
213 irinotecan network uses the same algorithm and constraints as the core clock model, see **Supplementary**
214 **Information**. The cost function is extended to account for the additional genes in the network.

215 The model variables representing proteins relevant for irinotecan PK-PD, *i.e.* UGT, CES, ABCB and
216 ABCC, do not regulate gene expression within our transcription translation network and are thus not
217 constrained by the experimental data used for the model fit. Maximal protein concentration for UGT,
218 CES, ABCB and ABCC are scaled to the maximal concentrations used in the original model. As the
219 protein concentrations predicted by the transcription-translation network are rescaled, the prediction of
220 toxicity is based on the relative amplitude and the phase of the protein oscillations, but not on their
221 absolute levels. The model of Dulong *et al.* 2015 [27] explicitly involves ABCG, which is in our case
222 replaced by ABCC with an appropriate rescaling, and it uses protein dynamics that result from a fit of a
223 cosine curve to protein data. We replaced the cosine fit with the dynamics that result from the clock-
224 irinotecan network. For the cell line Caco-2 (cell line derived from a human colorectal adenocarcinoma),
225 the PK-PD model was fitted to cell death following irinotecan treatment [26, 27]. To fit the circadian
226 variation in toxicity, we change the PK-PD model output by replacing the equation modelling apoptosis
227 with two equations for the time series of proliferation and cytotoxicity, see **Supplementary Equations**
228 **(3.29)** and **(3.30)**. As it turns out, the changes in the model due to treatment are not sufficient to explain
229 the large differences observed experimentally, likely due to the small relative amplitudes of the protein
230 oscillations, which in our model is defined by **Supplementary Equations (3.1)** to **(3.19)** and cannot be
231 larger than the fitted mRNA oscillations. To relax this constraint, we replace constant protein degradation
232 for UGT, CES, ABCB and ABCC with oscillatory degradation [36]. Abundances of dead cells are
233 measured experimentally as red florescent objects. To prevent dependence on initial conditions, the
234 cytotoxicity curves are all shifted along the cytotoxicity axis such that the first value of all curves overlaps
235 with the control curve.

236 For convenience, acrophases are rescaled to the range from 0 to 1 instead of 0 to 2π .

237

238 2.8 Statistical analysis

239 The experimental toxicity profile is fitted by a harmonic regression using matlab, significance is set to
240 $p \leq 0.05$. The Area Under the Curve is calculated using the linear trapezoidal method, using as weights w_k
241 a vector with n elements (where n is the number of time points considered), with 1 hour for the first and
242 last element, and 2 hours for the other elements, with the error associated calculated as $var(AUC) =$
243 $\sum_{k=0}^{n-1} w_k^2 SEM_k^2$,

244 where SEM_k is the standard error at the time point related to time point k , and var is the variance of the
245 AUC calculated as $AUC = \sum_{k=0}^{n-1} w_k x_k$.

246

248 3. Results

249 The effect of a drug results from an intricate interplay between its metabolites and the organism, which
250 is under circadian control. Regarding the anticancer agent irinotecan, multiple genes and proteins
251 involved in its PK-PD are directly or indirectly regulated by the cellular core clock. The aim of the study
252 was to design a mathematical model combining the core clock and irinotecan PK-PD-related elements to
253 investigate possible cellular biomarkers predicting irinotecan chronotoxicity rhythms (**Fig. 1a**, top). This
254 model was developed and calibrated for three biological systems: the healthy mouse liver, and two cell
255 lines derived from human colorectal cancer (CRC) (**Fig. 1a** bottom). The combined model was trained
256 for the CRC cell lines using circadian datasets of mRNA levels and with experimental results on time-
257 related irinotecan cytotoxicity. We first present a quantitative version of the core-clock model (**Fig. 1b**),
258 followed by its extension to account for the clock-controlled regulation of genes involved in irinotecan
259 PK-PD. Finally, this model was connected to a representation of irinotecan chronoPK-PD.

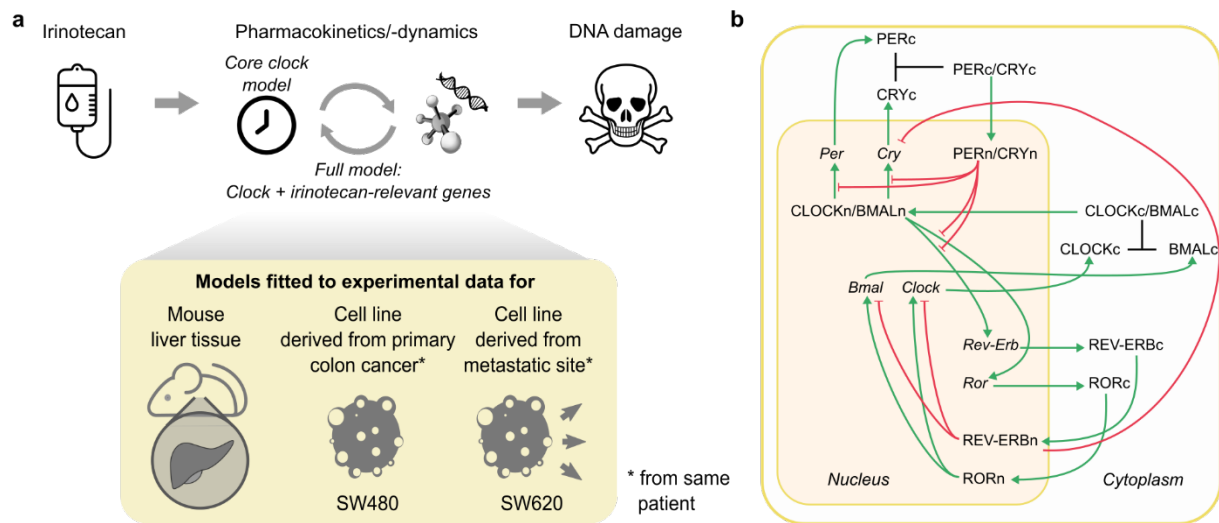
260

261 3.1 A quantitative model of the core clock in mouse liver

262 To investigate the interactions between the circadian clock and the irinotecan cellular PK-PD, we started
263 by designing a quantitative model of the cellular core clock (**Fig. 1b**). We used the previously published
264 ODE model by Relógio *et al.* [23], which represents the molecular mechanisms of the core clock at the
265 cellular level based on experimental data for the mammalian SCN. Clock gene paralogs and isoforms
266 were merged into the following model variables for mRNA elements: *Per* (*Per1*, *Per2*, *Per3*), *Cry* (*Cry1*,
267 *Cry2*), *Ror* (*Rora*, *Rorb*, *Rorc*), *Rev-Erb* (*Rev-Erba*, *Rev-Erb β*) and *Bmal1*. We applied the same principle
268 for model variables representing proteins and protein complexes. The dynamical variable
269 CLOCK/BMAL representing the CLOCK/BMAL1 dimer is assumed to activate the transcription of the
270 core-clock genes *Rev-Erb*, *Ror*, *Per*, and *Cry* and the PER/CRY complex to inhibit this transcriptional
271 activity. The model includes two main negative feedback loops. The first one involves the self-inhibition
272 of the dynamical variable *Per* and *Cry* through the inhibition of CLOCK/BMAL by the PER/CRY
273 complex. In addition, REV-ERB inhibits the transcription of *Cry*, thus inhibiting its own inhibition
274 through the regulation of PER/CRY. The second feedback loop is induced by the self-repression of the
275 dynamical variable *Bmal* through the activation of its repressor REV-ERB by CLOCK/BMAL. Contrary,
276 ROR, which is transcriptionally activated via CLOCK/BMAL, acts positively on *Bmal* regulation.
277 The Relógio *et al.* model differentiated between phosphorylated and unphosphorylated PER proteins
278 [23]. However, in the absence of time-dependent quantitative data on PER phosphorylation, we opted to
279 simplify the PER/CRY (PC) loop and to merge the phosphorylated/unphosphorylated variables (**Fig. 1b**).
280 Similarly, the equations for the dynamical variables CLOCK/BMAL and PER/CRY cytoplasmic
281 complexes originally included both a term for complex dissociation into free proteins and for complex
282 degradation, which were not identifiable from the available data so that the degradation terms were
283 removed (**Supplementary Information, Section 1**).

284 We further refined the core-clock model to represent the core clock in organs relevant for irinotecan
285 pharmacology, in particular the liver, where the drug is processed. The Relógio *et al.* model did not
286 explicitly consider *Clock* given its lack of rhythmicity in the SCN [37]. However, this is not the case in
287 the liver [38]. Moreover, CLOCK/BMAL1 is a key transcriptional regulator of genes involved in the
288 irinotecan network [39, 40]. Thus, we expanded the initial model by explicitly including *Clock* as follows.
289 Similarly to the dynamical variable *Bmal*, *Clock* transcription is assumed to be positively regulated by
290 ROR and negatively impacted by REV-ERB [41]. The cytoplasmic protein CLOCK_C dimerizes with the
291 dynamical variable BMAL_C and translocates to the nucleus to form the heterodimer complex
292 CLOCK/BMAL_N. The dynamical variable CLOCK_C representing the cytosolic CLOCK protein is

293 assumed not to be able to enter the nucleus, as it was not detected in the nucleus of cells not expressing
 294 *Bmal1* [42]. Of note, BMAL1 and CLOCK nuclear protein expressions shared the same circadian phase
 295 and amplitude experimentally, suggesting that both species exist mostly as dimers in the nucleus [43]
 296 (**Fig. 1b**). One last modification was made to the model structure to increase the accuracy of
 297 cytoplasm/nucleus transport terms. The equations now account for the ratio between the compartment
 298 volumes to ensure that the quantity of matter is conserved during transport (**Supplementary**
 299 **Information, Section 1.1.5**). The cytoplasm/nucleus volume ratio was set for mouse hepatocytes to 14
 300 [44].
 301
 302



303

304 **Fig. 1: The action of the drug irinotecan involves the core clock and a set of clock-regulated genes, experimentally**
 305 **assessable in different cell types. a** Workflow of the clock-irinotecan model construction. Irinotecan induces DNA damage
 306 and potentially cell death via its interaction with clock-controlled proteins. Mathematical models were fitted to different data
 307 sets in healthy mouse liver, and in human cancer cell lines. **b** Network representation of the core-clock model. Inhibitory
 308 interactions are presented in red with flat arrowheads, activating interactions in green, and complex formation in black.

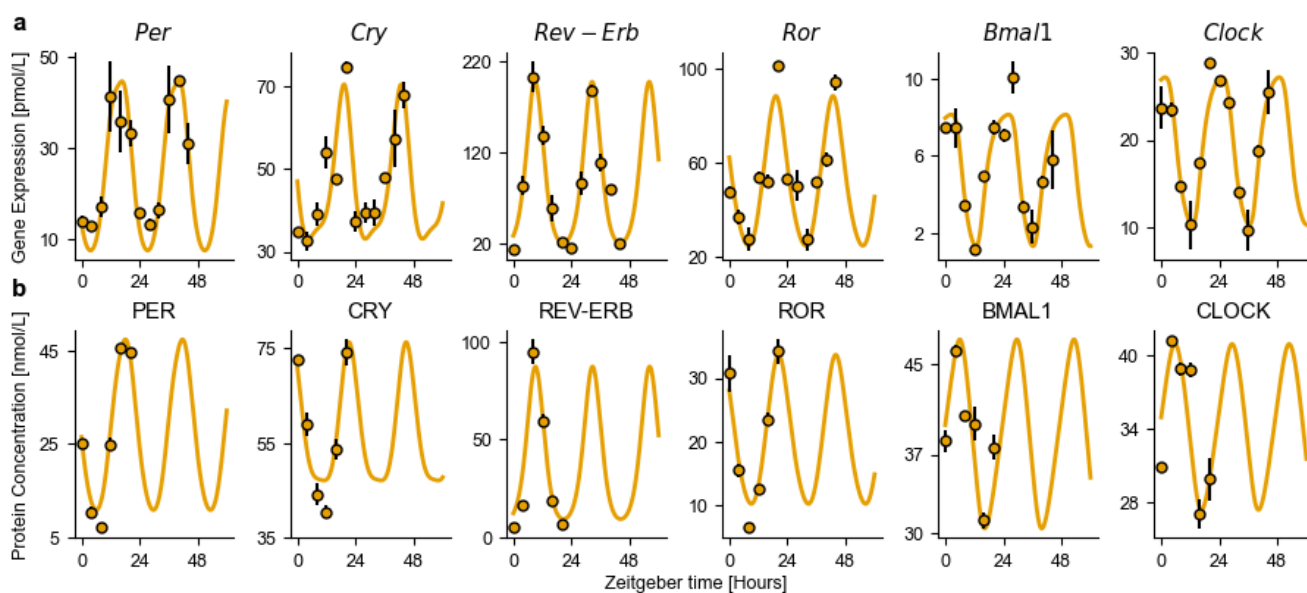
309

310 Our new core-clock model allows to quantitatively simulate gene and protein levels, expressed in mol/L,
 311 thus allowing for the fitting of quantitative datasets informing on absolute concentrations. Parameter
 312 estimation was done using the time series data reported by Narumi *et al.* [38] (**Supplementary**
 313 **Information, Section 1.3.4**). Starting from the Religio *et al.* model, we performed a linear change of
 314 variables, mapping the original model variables to their scaled versions with respect to the maximum of
 315 the observed data (**Supplementary Information, Section 1.3.2**). The obtained scaled parameter values
 316 were then used as an initial guess for the subsequent parameter estimation procedures.

317 The liver data set also included protein expression for *Bmal1*^{-/-} mice [38]. Assuming that *Bmal1* knockout
 318 (KO) led to a loss of oscillations in the clock [45], this data could be seen as a glance at the system at
 319 steady state. This enabled us to derive functional relationships to compute three transcription rate
 320 parameters as a function of the KO mice and other parameters (**Supplementary Information, Section**
 321 **1.3.3**), thus decreasing the number of parameters to estimate. This led to a simplification in the parameter
 322 estimation. We further reduced the number of parameters by assuming that Hill power coefficients were
 323 equal for all activators (parameter *b*) and all inhibitors (parameter *c*) of the transcription across genes.

324 This led to a decrease of 8 parameters to be estimated while producing next to no change in the goodness
 325 of fit as expected from the argument of unidentifiability. Only *Cry* kept separated Hill coefficients due
 326 to its transcription being regulated by 3 species (the dynamical variables CLOCK/BMAL, PER/CRY and
 327 REV-ERB). The final core-clock model has 18 state variables and 58 parameters to be estimated.
 328 The parameter estimation procedures consisted in a numerical minimization of a cost function, which
 329 was the sum of two terms (**Supplementary Information, Section 1, Equation (1.28)**). The first term is
 330 the least square error between the data and the model's simulation, while the second term accounts for
 331 biological constraints. These constraints were derived from co-immunoprecipitation experiments and
 332 provided bounds for complex concentrations with respect to free protein concentrations [42, 46].
 333 Additional constraints were specified on the bounds of parameter search intervals including those of
 334 degradation or transcription rates based on mRNA and protein half-lives and levels [47]. **Fig. 2** shows
 335 the model best-fit, which convincingly reproduced the data ($R^2 = 0.86$). *Bmal1* and *Clock* mRNA model-
 336 predicted profiles presented a similar phase but different mean levels (5.3 and 19.5 pmol/L, respectively)
 337 and relative amplitude (84% and 62% of the mean, respectively). Differences were also observed at the
 338 protein level as free BMAL1 and CLOCK protein mean levels were equal to 13.9 and 8.85nmol/L
 339 respectively, with relative amplitudes of 35% and 25%. These differences came as a justification to the
 340 addition of the *Clock* gene into the core-clock model.

341



342

343 **Fig. 2: Best fit of the quantitative core-clock model to mRNA and protein circadian datasets in the mouse liver. a**
 344 **mRNA expression for core-clock elements in pmol/L. b Protein levels for core-clock elements in pmol/L. Model simulation**
 345 **(orange lines), experimental data used for calibration (black circles). Depicted are mean values ($n = 2$ biological replicates) \pm**
 346 **SEM.**

347

348 Validation of the model was done using an external time course dataset from mouse hepatocytes, which
 349 was not used for the model design and calibration [43]. This study reports a phase between 8.5h and
 350 10.8h for the circadian rhythm of REV-ERB nuclear expression and a relative amplitude of 98%, while
 351 the model simulation for phase and relative amplitude were 9.7h and 90%, respectively. Similarly, for

352 ROR nuclear expression, the reported phase was 20.8h, as compared to 21.1h for model predictions, and
353 its relative amplitude was 80% as compared to 69% for the model. Both predictions are in close
354 agreement with the study and serve as a validation of the model. For the other clock proteins, as our
355 model only tracked them as complexes in the nucleus, the comparison to data was not possible. A
356 subsequent robustness analysis was performed by analyzing whether the model could maintain sustained
357 oscillations upon parameter perturbation. Gaussian noise was added to the best-fit parameter vector with
358 a standard deviation of 10%, leading to oscillating simulations in 73% of the cases, thus demonstrating
359 the model robustness (**Supplementary Fig. 1**).

360

361 3.2 The clock model reproduces the expression profiles of core-clock genes in CRC cell lines

362 To test our mathematical model in a colon cancer context, we chose a well-known *in vitro* cellular model
363 of CRC progression, which includes two cell lines from the same patient (SW480, SW620), derived from
364 the primary tumour and from the metastasis, respectively. We carried out a time course of 45 hours (9h
365 - 54h after synchronization) with a 3 hours sampling interval, for the gene expression analysis of *PER2*,
366 *REV-ERB α* and *BMAL1* via RT-qPCR, in either control or sh*BMAL1* conditions. This dataset was
367 combined with microarray data for the expression of *Cry*, *Ror* and *Clock* in order to calibrate the core-
368 clock model for each of the CRC cell lines (**see section 2.6**). Quantitative mean concentration levels
369 expressed in mol/L for the clock genes of CRC cell lines were derived from an already published RNA-
370 seq transcriptomic dataset [11]. Thus, in total, three datasets were combined for the calibration of the
371 core-clock model for the CRC cell lines. The transcription-translation network was assumed to be similar
372 in either control or sh*BMAL1* conditions, yet with a different parameter to account for sh*BMAL1* activity.
373 Accordingly, the RT-qPCR datasets obtained from the control and sh*BMAL1* conditions were fitted
374 simultaneously to their respective models using the same set of parameter values with the exception of
375 *BMAL1* basal transcription, which was allowed to differ between both conditions (**Supplementary Fig.**
376 **3**). The sh*BMAL1* condition provided a view of a dampened circadian clock, due to the knockdown of
377 *Bmal1*, which induced a lower activation power of the transcription factor CLOCK/BMAL1. Upon model
378 calibration, a 375-fold reduction in the *BMAL1* estimated basal transcription rate was necessary to allow
379 for a good fit of both conditions. This demonstrates the ability of the model to reproduce two different
380 physiological scenarios by tuning a single parameter.

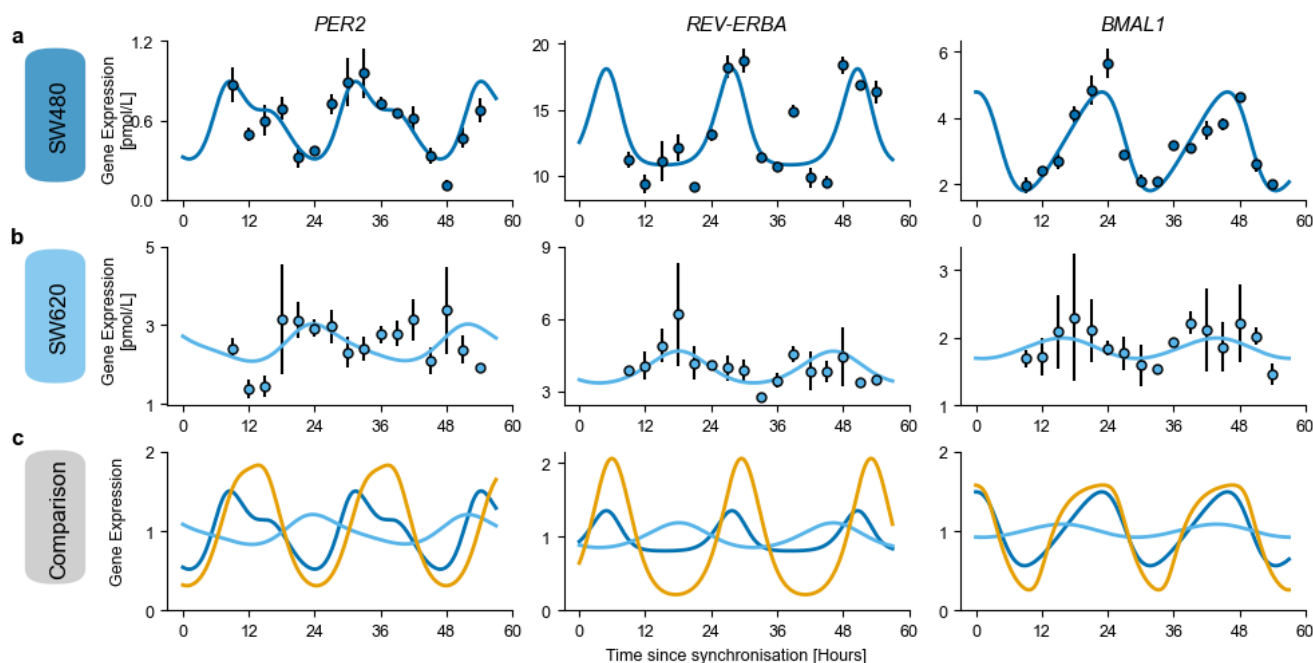
381 Concerning the SW480 cell line, the model achieved an excellent fit of the data ($R^2 = 0.75$) (**Fig 3a,**
382 **Supplementary Fig. 2a**). The fit for the SW620 was reasonable as well ($R^2 = 0.67$), but lacked a proper
383 fit of *CRY*, *ROR* and *CLOCK* expression reported in the microarray dataset (**Fig 3b, Supplementary**
384 **Fig. 2b**). Oscillations of the core-clock genes, normalized to the mesor, showed larger relative amplitudes
385 in the healthy mouse liver than in CRC-derived cell lines, with the circadian rhythms in SW620 cells
386 being largely dampened as compared to both other systems (**Fig. 3c**). The peaks of *BMAL1* mRNA levels
387 of the best-fit model for mouse liver and SW480 cells were aligned to allow for an *in vitro/in vivo* systems
388 comparison. This highlighted a moderate phase shift in *PER2* and *REV-ERBA* gene expression of 5 hours,
389 and less than 1 hour in *BMAL1* expression between the SW480 cell line and liver tissue. On the opposite,
390 larger phase delays were observed in the case of the SW620 cell line. Although the three models represent
391 different organs in different conditions, their comparison exhibited a moderate agreement between the
392 clocks of the healthy liver and of the SW480 colorectal cancer cell line, and large differences in terms of
393 oscillation dampening and phase differences in comparison to the clock of the SW620 metastatic colon
394 cancer cell line.

395 For most core-clock genes, the oscillations displayed a non-cosine shape, with longer intervals of high
396 gene expression for *PER2*, *BMAL1* and *CLOCK* compared to *REV-ERBA* and *CRY*. Overall, the here

397 presented core-clock model, based on cellular mRNA and protein concentrations, reproduced the
398 circadian gene expression profiles for different sets of experimental data with good precision. Thus, this
399 model provided a reasonable starting point for the following extension with irinotecan PK-PD-related
400 genes.

401

402



403

404 **Fig. 3: Comparison of the core-clock models fitted to healthy mouse liver or human cancer cell lines.** Best fit of the
405 quantitative core-clock model to (a) the SW480 cell line and (b) the SW620 cell line. Model simulation (line) against the RT-
406 qPCR data used for calibration (dots), depicted are mean values ($n = 3$) \pm SEM. c Comparison of the model fit for liver
407 (orange), SW480 (dark blue) and SW620 (sky blue). *Bmal1* circadian phases were aligned for mouse liver and SW480 cell
408 line, and all gene expression profiles were normalized to the mesor to allow for comparison. See **Supplementary Fig. 2**
409 for the other genes of the core clock model.

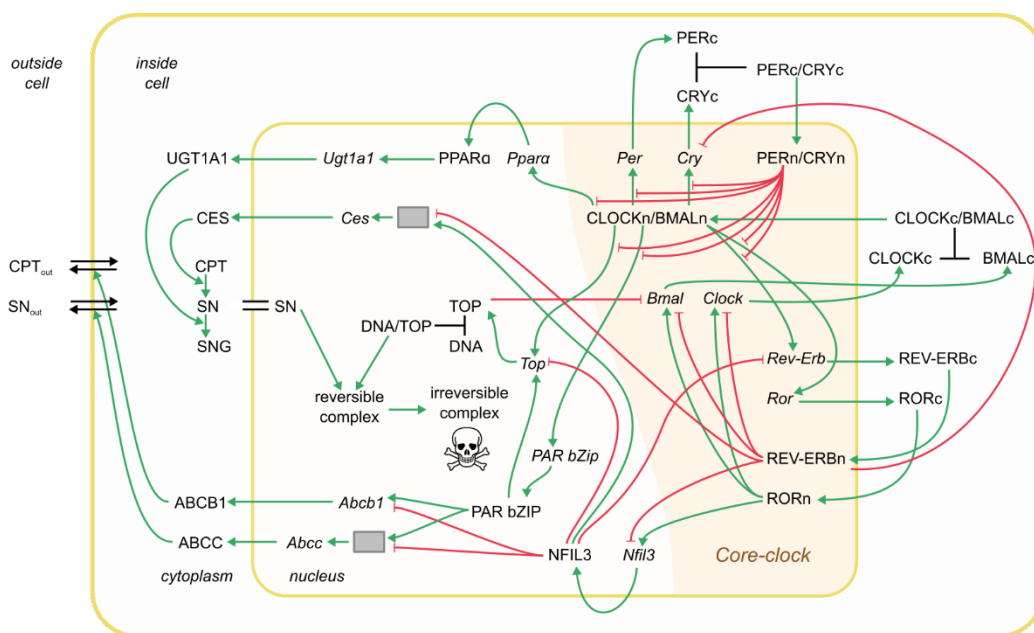
410

411 3.3 Filling the gap: connecting the core clock with irinotecan PK-PD related genes

412 We extended the core-clock network with eight clock-controlled genes relevant for irinotecan
413 pharmacology as depicted in **Fig. 4**, named in the following clock-irinotecan network. The elements
414 added to the core-clock model are involved in irinotecan metabolism, transport, and pharmacodynamics.
415 Irinotecan is a prodrug, which needs to be converted into its active metabolite, SN-38, through the
416 enzymatic activity of CES2 (Carboxylesterase 2) [48]. Subsequently, UGT1A1 (uridine diphosphate
417 glucuronosyltransferase 1) regulates the conversion of SN-38 into its inactivated form, SN-38G [28]. The
418 ATP-Binding Cassette (ABC) transporters ABCB1, ABCC1, ABCC2 and ABCG2 control the efflux of
419 these molecules out of the cells [49]. Central to irinotecan action, SN-38 binds to the protein TOP1 (DNA
420 topoisomerase 1), which under normal conditions releases the supercoiling and torsional tension of DNA
421 by transiently cleaving and rejoining one strand of the DNA, thereby controlling DNA topology during
422 replication and transcription. SN-38 binds to the DNA-TOP1 complexes to stabilize them. This leads to

423 double-stranded breaks, erroneous transcription and likely cell death [50, 51]. Besides these proteins
 424 directly relevant for irinotecan PK-PD, the clock-irinotecan network contains three elements that act as
 425 transcription factors for the above-mentioned genes, DBP (D site of albumin promoter (albumin D-box)
 426 binding protein), which is also considered as a core-clock element, NFIL3 (Nuclear factor, interleukin 3
 427 regulated), and PPARA (Peroxisome proliferator-activated receptor alpha), a regulator of liver lipid
 428 metabolism that also acts as transcription factor for UGT1A1, which deactivates SN38 [52-54]. For the
 429 clock-irinotecan network, we only consider the ABC transporter ABCB1 for irinotecan efflux and
 430 ABCC1 for SN38 and SN38G efflux as *ABCC2* showed less clear circadian oscillations and *ABCG2* did
 431 not appear in our RNA-seq data for the studied cell lines. The mathematical description of the clock-
 432 irinotecan network contains 39 equations and 115 parameters (**Supplementary Table 5 and 6,**
 433 **Supplementary Equations (3.1) - (3.19)**). In the clock-irinotecan network, oscillations are inherited
 434 from the core clock to genes outside of the core-clock network via the CLOCK/BMAL1 complex, ROR
 435 and REV-ERB. Accordingly, most connections go from core clock to the remaining elements. Only the
 436 inhibition of *REV-ERB* by NFIL3 and the inhibition of *BMAL1* by TOP1 provide a feedback from the
 437 irinotecan-related genes to the core clock [55, 56]. From the clock-irinotecan network fitted to
 438 experimental mRNA expression data, we use the mRNA dynamics of *UGT1A1*, *CES2*, *ABCB1* and
 439 *ABCC1* as an input to the protein dynamics and the PK-PD model to predict irinotecan toxicity, see
 440 below.

441



442

443 **Fig. 4: Model of the interplay between irinotecan PK-PD and the core clock.** Irinotecan treatment is simulated
 444 by a transcriptional-translational network that comprises the core clock, irinotecan-relevant genes, and the PK-PD
 445 of irinotecan. Different types of interactions are represented among the elements of the network: inhibition (red
 446 arrows with flat arrowhead) and activation interactions (green arrows); complex formation (black lines). Grey
 447 boxes represent post-transcriptional sub-networks necessary for a model fit to the data. The double black line
 448 indicates equal concentrations between nucleus and cytoplasm, the double black line with arrowheads indicates
 449 CPT-11 and SN-38 cellular transport inside and outside of the cell. All indicated molecular interactions are based

450 on experimental evidence from a number of different sources and corresponding references are provided in
451 **Supplementary Table 3.**

452

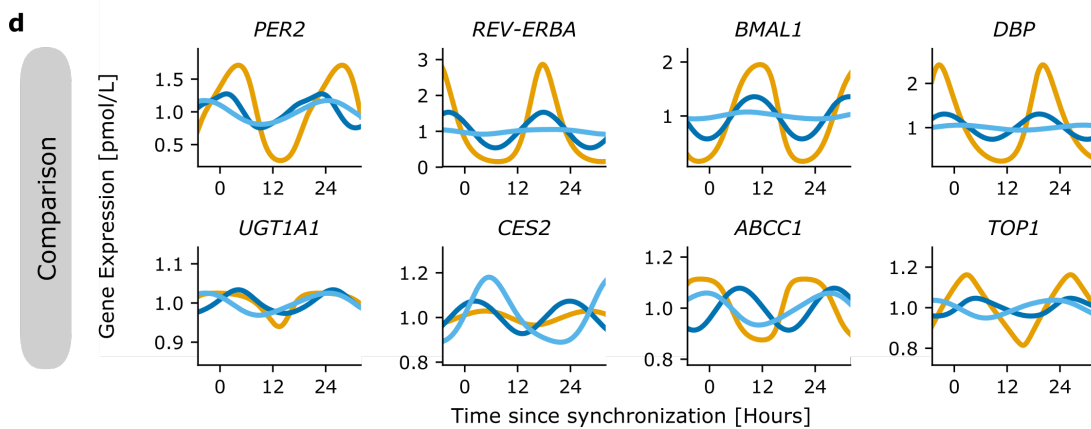
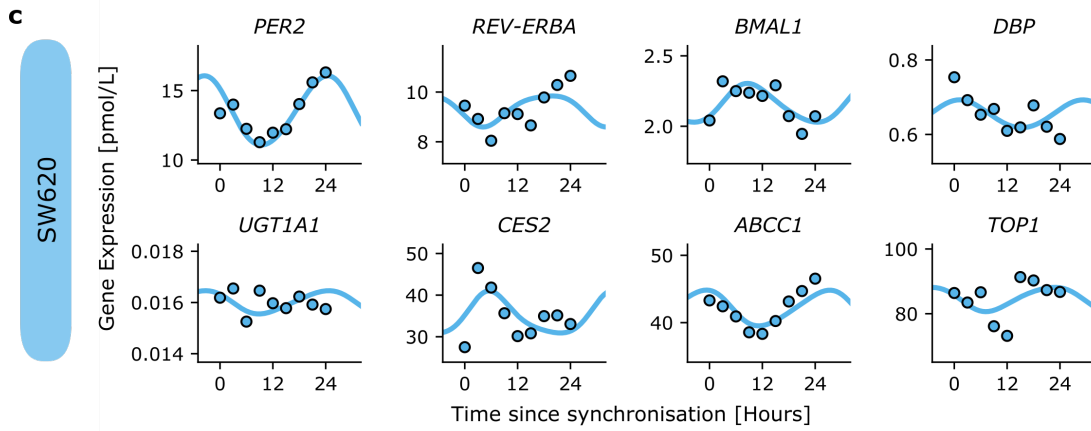
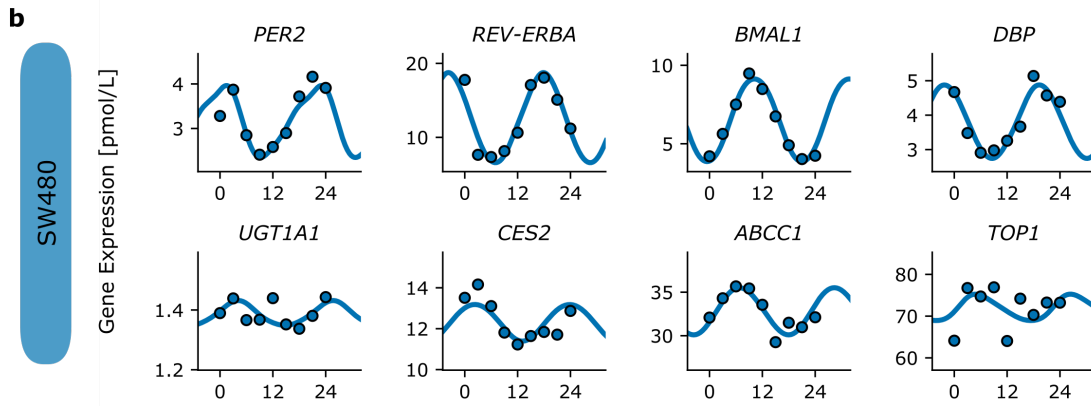
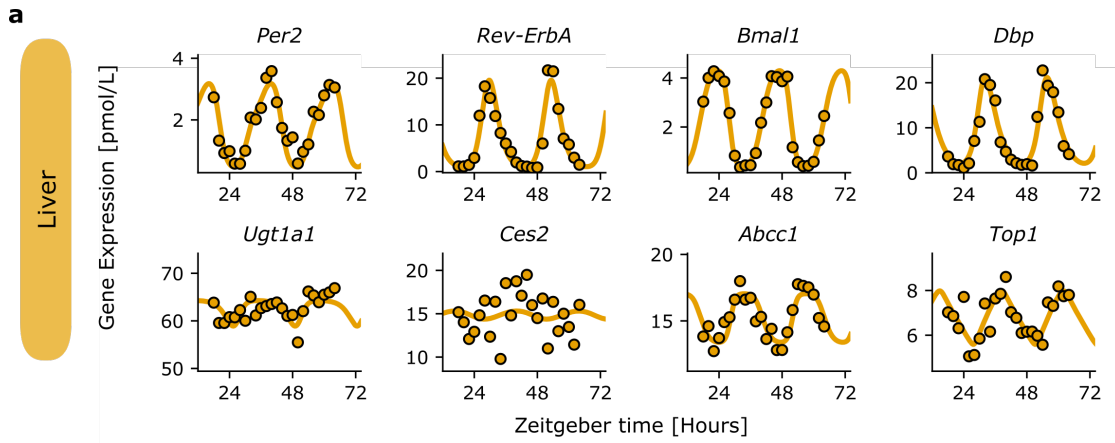
453 The clock-irinotecan network was fitted to experimental time-series data sets of mRNA concentrations
454 [34], available for mouse liver [11] and extracted from microarray and RNA-seq data for CRC cell lines,
455 see section 2 for details. We fitted the clock-irinotecan model to the temporal dynamics of mouse liver,
456 as well as to untreated SW480 and SW620 cells, which resulted in R^2 scores of 0.72, 0.61 and 0.40,
457 respectively (**Fig. 5a-c**), see **Supplementary Fig. 4** for an example with all genes. For acrophases and
458 relative amplitudes of the model fits see **Supplementary Fig. 5**. Periods predicted by the model are 23.5h
459 for the liver (in accordance with literature values for the circadian period of mice [57]), 21.6h for the
460 SW480 cells and 28.8h for SW620 cells (within the range of previously reported values [17, 30]).

461 A first version of the model assumed direct (i.e. one step) regulation of irinotecan-related gene
462 transcription by elements of the core clock (**Supplementary Equations (3.1) to (3.12)**, i.e. **Fig. 4** without
463 the grey boxes). While this restriction did not hamper the fitting of most genes, the resulting best-fit
464 curves for *CES2* and *ABCCI* mRNA levels were phase shifted compared to corresponding microarray
465 data in SW cell lines. This originated from large phase delays between the clock-controlled regulators
466 and the expression of the regulated genes. For example, *CES2*, which showed clear circadian oscillations
467 in the SW480 cell line (harmonic regression for a 24 h period results in p -value=0.014, acrophase=0.09
468 $\text{rad}/2\pi$, relative amplitude=30%), peaked seemingly before its two regulators, *REV-ERBA* and *NFIL3*,
469 see **Supplementary Fig. 5**. Thus, more intermediate elements might play a role in the network. As a
470 simple solution, we extended the model for *CES2* clock-controlled transcription by a simple chain of
471 post-transcriptional modifications, compare **Supplementary Equations (3.13) to (3.19)** and see **Fig. 4**,
472 grey boxes; to cover the phase delay between *Ces2* and *NFIL3* of 0.60 $\text{rad}/2\pi$ (12.9 hours, phase delay
473 between *Ces2* and *REV-ERBA* is 0.85 $\text{rad}/2\pi$, i.e. 18.2 hours), three unidirectional activation steps with
474 one parameter for both activation and degradation rates were required. As *ABCCI* showed a similar
475 problem, we added an analogue set of intermediate reactions for *ABCCI* transcription, for which two
476 steps were sufficient, as the phase delay with its regulators was smaller (phase delay between *Ces2* and
477 *NFIL3* of 0.39 $\text{rad}/2\pi$, i.e. 8.4 hours, phase delay between *Ces2* and *REV-ERBA* of 0.64 $\text{rad}/2\pi$, i.e. 13.8
478 hours), see **Supplementary Fig. 5**. The fit of the additional genes does not reduce the quality of the fit
479 of the core-clock model, with R^2 scores for the core clock of the full fit of 0.93, 0.78 and 0.57 compared
480 to 0.84, 0.67 and 0.52 for a fit of only the core clock using the rescaled microarray data (see section 2),
481 for liver tissue, SW480 and SW620 cell lines, respectively. Lower R^2 scores for the full fit likely result
482 from the longer optimization required for a good fit of all genes compared to the optimization required
483 for fitting only the core clock genes. From liver to SW480 to SW620, the relative amplitude of the
484 oscillation was reduced for genes of the core clock and for genes directly regulated by the core clock,
485 whereas this amplitude reduction was relaxed for genes only indirectly controlled by the core clock (**Fig.**
486 **5d** and **Supplementary Fig. 5b**).

487 From the fit of the gene expression data, we obtained a calibrated model computing clock and irinotecan-
488 related mRNA circadian rhythms. However, mRNAs need to be translated into proteins that eventually
489 interact with the drug. Hence, the link between the clock-irinotecan network and the PK-PD model for

490 treatment toxicity was assumed via the protein dynamics and allows us to investigate the interplay
491 between the circadian clock and irinotecan action. We designed a new model of protein dynamics of
492 UGT1A1, CES2, ABCB1 and ABCC1, which are the inputs for the irinotecan chronoPK-PD model
493 (**Supplementary Equation (3.3) with (3.29)**), replacing the forced cosine function utilized in the
494 original model by Dulong *et al.* 2015 [27]. The protein dynamics include a circadian degradation as
495 common for many proteins [36]. Magnitude, amplitude and phase of the circadian degradation are fitted
496 to cytotoxicity data; the translation rate is set to 1 as protein abundances are re-scaled in the PK-PD
497 model, see section 2 [36].

498



500 **Fig. 5: Comparison of the fitted clock-irinotecan network for healthy mouse liver and human cancer-**
501 **derived cells.** Selected gene expression and fit of the clock-irinotecan network for (a) mouse liver data, (b) SW480
502 and (c) SW620, all data without treatment. d Comparison of the model output when fitted to liver (orange), SW480
503 (dark blue) and SW620 (sky blue). Profiles were normalized to the mesor, and *BMAL1* phases were aligned
504 between mouse liver and the SW480 cell line to allow for comparison.

505

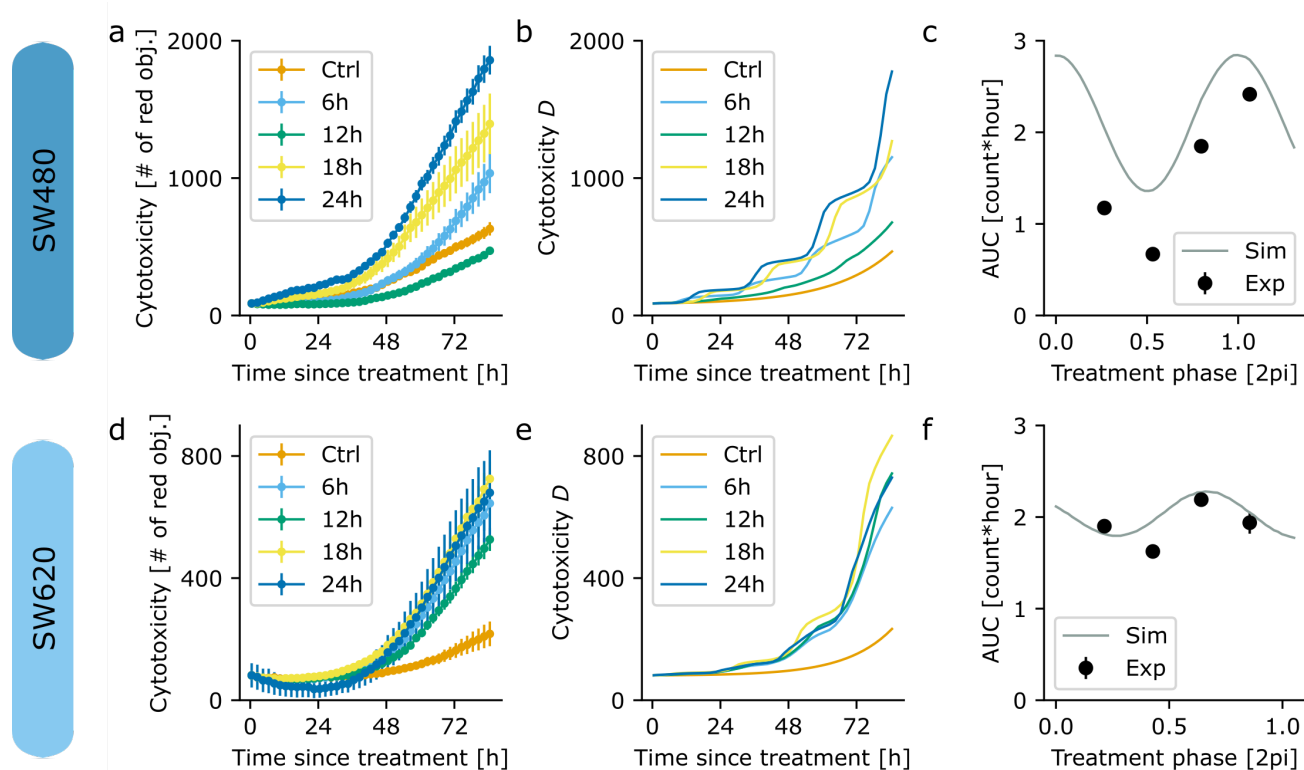
506 3.4 The full clock-irinotecan model recapitulates different chronotoxicity rhythms for CRC cells

507 To investigate the putative effects of time-dependent treatment in CRC, SW480 and SW620 cells were
508 synchronized by media change and treated with 2 μ M of irinotecan at four different circadian times (CT
509 after synchronization: 6h, 12h, 18h and 24h). The SW480 cell line exhibited a circadian cytotoxicity
510 response to treatment (harmonic regression with the period of the model fit, $p = 0.043$ for SW480, see
511 **Supplementary Fig. 7**; not significant for SW620). SW480 cells showed the highest toxicity when
512 irinotecan was administered 24h after synchronization, while the lowest toxicity was observed when
513 irinotecan was administered 12h post synchronization (acrophase of $0.006 \pm 0.03 \text{ rad}/2\pi$, **Fig. 6 c**). The
514 differences in cytotoxicity values between different treatment time points were higher in SW480 as
515 compared to SW620 cells, which resulted in larger circadian amplitudes for the SW480 toxicity rhythm
516 (**Fig. 6b**). Here it is relevant to notice that, in the absence of treatment, the number of dead cells in SW480
517 cultures is higher than for SW620 cell cultures (ratio of the area under the curve of SW480 and SW620
518 is 2.46 ± 0.07 , **Fig. 6 a and d**) pointing to cell death and cell cycle differences between the tumor and the
519 metastasis-derived cells, which might be due to their altered circadian clock.

520 To allow for the comparison of the model with this experimental data, we supplemented the model by
521 Dulong *et al.* 2015 [27] with two cell population equations that explicitly track the number of alive and
522 dead cells. An exponential growth and a first-order natural cell death were assumed in both control and
523 treated conditions. Irinotecan was assumed to act negatively on cell proliferation and survival through
524 DNA damage formation, and a circadian oscillation in the cell death rate was added, see **Supplementary**
525 **Equations (3.30) and (3.31)**. Parameters of the original model were kept unchanged apart from the
526 formation rate of the irreversible complex, which had to be adapted for a successful fit, and which ended
527 up being reduced as compared to its former estimation.

528 Using the mRNA dynamics computed by the clock-irinotecan model, the irinotecan PK-PD model allows
529 to derive a prediction of the circadian dynamics of cell death (**Fig. 6**). The best-fit full model generated
530 a prediction that agreed with the toxicity phase of the experimental data for the SW480 cell line. The
531 model also recapitulated a different toxicity profile for the SW620 cell line, supporting the hypothesis
532 that the same drug at the same concentration could lead to different responses based on the time of
533 treatment administration and on the cancer clocks. Interestingly, while the highest and lowest cytotoxicity
534 trends were the same in both cell lines, the overall response to the cytotoxic effect of the drug was higher
535 in SW480 (derived from the primary tumour) in comparison to SW620 (derived from a metastasis, but
536 from the same patient). This also alludes to a role of the cellular clock profile in treatment outcome, as
537 the two cell lines have different oscillatory patterns. We further tested a simplified version of the equation
538 for the protein dynamics assuming constant, i.e. non-circadian, protein degradation (**Supplementary**
539 **information, Equation (3.3)** with constant degradation rate). As anticipated by the mathematical

540 analysis, toxicity oscillation amplitudes were drastically reduced to approximately 1% of the mesor and
 541 were then much smaller than those observed experimentally. Yet, the clock-PK-PD model with minor
 542 adaptations to the experimental settings gave reasonable toxicity phases using non-circadian protein
 543 dynamics with an appropriately chosen degradation rate (**Supplementary Fig. 6**), without fitting the
 544 model to the circadian toxicity values obtained experimentally, see **Supplementary Fig. 7**.
 545



546
 547 **Fig. 6: Fitting of the time-dependent treatment from human cancer cell lines.** **a** Experimentally measured cytotoxicity
 548 curves, estimated by measuring red fluorescent objects (see Methods), for SW480 cells that are untreated (Ctrl), or treated at
 549 indicated time points with irinotecan (6h, 12h, 18h or 24h after synchronization). Time is aligned to treatment onset. **b** Best-
 550 fit of the extended PK-PD model (shown is the number of dead cells, the dynamical variable D of Supplementary Equation
 551 (3.31)) to the experimental cytotoxicity data of the SW480 cell line. **c** Area Under the Curve (AUC) of treated SW480 cells
 552 normalized by the untreated control (dots), compared with the area under the curve of the best-fit model (grey line). **d**
 553 Experimentally measured cytotoxicity curves for SW620 cells untreated (Ctrl), or treated at indicated time points with
 554 irinotecan (6h, 12h, 18h or 24h after synchronization). **e** Best-fit of the extended PK-PD model to the experimental cytotoxicity
 555 data of the SW620 cell line. **f** Area under the curve of treated SW620 cells normalized by the untreated control (dots),
 556 compared with the area under the curve of the best-fit model (grey line).

557
 558 To test for the sensitivity of our final model to parameter variations, we evaluated parameter sensibility
 559 of a set of 123 parameters with respect to the phase and amplitude of the irinotecan circadian toxicity
 560 profile (i.e. the curves depicted in **Fig. 6c** and **f**) by calculating Sobol sensitivity total order indices, see
 561 **Supplementary Fig. 9**. A close agreement was found between the parameter sensitivity on the phase and

562 on the amplitude of the drug chronotoxicity rhythms. Our analysis highlighted the impact of the protein
563 dynamics on the toxicity profile, most importantly the relevance of the phases of the circadian
564 degradation of CES2 (parameter ϕ_{Ces} from **Supplementary Fig. 9**) and UGT1A1 (parameter ϕ_{Ugt})
565 and the amplitude of CES2 (parameter amp_{Ces}). Besides those parameters, several core-clock elements
566 - in particular parameters associated with the loop formed by *ROR*, *BMAL1* and *CLOCK* (maximal
567 transcription rates, degradation rates, production rates) - showed high sensitivity, probably because
568 existence of oscillations depends on the core clock. The feedback from irinotecan-relevant genes to the
569 core clock, through the inhibition of *REV-ERB* by NFIL3 (parameter $i_{RevNfil}$) and the inhibition of
570 *BMAL1* by TOP1 (parameter $i_{BmalTop}$), only showed a weak impact on the toxicity curve. All
571 parameters associated with ABC transporters showed a low impact on the toxicity profile.

572

573 **4 Discussion**

574 The circadian clock regulates the timing of various crucial molecular pathways including drug
575 metabolism, apoptosis, DNA damage repair and cell cycle [58-60]. The malfunctioning of these
576 pathways is involved in cancer onset and progression. On the other hand, several drugs used in cancer
577 treatment target genes, which are expressed in a circadian manner and also the metabolism of these drugs
578 is carried out by circadian-regulated genes and proteins. Hence, timing treatment in accordance with the
579 patient's circadian timing system is likely to contribute to improved treatment outcome, and several
580 studies have shown promising results using chronotherapy in cancer treatment [8].

581 We developed a novel mathematical model of irinotecan cellular PK-PD, which links the core clock with
582 predicted treatment toxicity for CRC cells. The model simulations highlighted the existence of time-
583 dependent toxicity for the different cells, which was different for the tumour-derived cell line as
584 compared to the metastasis-derived cell line. Our results suggest that, in addition to gene expression, the
585 dynamics of protein translation, with circadian variation in the degradation, plays an important role in
586 the timing of drug toxicity. In particular the phase (the time of maximal expression) and amplitude
587 (difference between minimal and maximal normalized expression) of the circadian oscillation in protein
588 degradation of CES2, which controls the activation of irinotecan, seems to be relevant in shaping the
589 toxicity profile. Moreover, elements associated with core-clock genes, such as *BMAL1* or *CLOCK*
590 showed high sensitivity which proved the importance of the core-clock parameters on irinotecan toxicity.

591

592 **4.1 A comprehensive mathematical model for circadian regulation of irinotecan PK-PD**

593 Our clock-irinotecan model can be fitted to different scenarios providing different circadian toxicity
594 profiles for CRC cells. The core-clock model was initially developed from multiple datasets of mammalian
595 SCN cells [23], and was successfully refined here using quantitative measurements of the clock of the
596 mouse liver, and of SW480 and SW620 cell lines. Regarding the model of irinotecan PK-PD, it was
597 designed based on extensive datasets in Caco-2 cells [27], and was further validated in both SW480 and
598 SW620 cell lines. Using SW480 and SW620 cell lines here provided a proof of principle that a
599 personalization of the model to other cell lines was possible. Hence, models of both the

600 transcriptional/translational clock network and irinotecan pharmacodynamics and -kinetics were
601 validated in several *in vitro* and *in vivo* experimental settings, which argues in favour of their reliability.
602 The reduction in fit quality from liver to SW480 to SW620 cells likely results from the decreasing
603 amplitudes of circadian oscillations [17, 30, 61], see also **Supplementary Fig. 5b**. Indeed, assuming that
604 the experimental data of the same gene, yet from different biological sources (liver or CRC cell lines),
605 shows the same level of noise, arising from biological stochasticity or from experimental constraints,
606 larger oscillation amplitudes lead to higher signal to noise ratios, which facilitates fitting. In addition, the
607 fact that the core-clock model did not fully fit the SW620 data was an indication that clock gene and
608 protein interactions may be impaired in this cell line or at least different from the ones implemented in
609 the model. It is also important to notice that each patient (or healthy individuals) and each cancer are
610 unique. Accordingly, also different cell lines, patients or healthy individuals [62] have specific clock
611 phenotypes, and this requires personalization of treatment [63]. Thus, any clinical application requires
612 that our model is fitted to the individual patient, or to a group of patients with similar clock molecular
613 profiles.

614 Another ODE-based model of the mouse liver clock was designed by Woller *et al.* to investigate the
615 effect of feeding cycles on liver circadian rhythms [64, 65]. That model was developed to address a
616 different question as compared to this study and could not be readily used here, as for instance the energy
617 metabolism part was out of the scope of this study. In addition, that model did not include different
618 compartments for the nucleus and the cytoplasm, which we were able to precisely do thanks to the recent
619 publication of data on clock-gene subcellular trafficking [43]. Further, we included the gene *Clock* to the
620 model, to incorporate available data on this gene and investigate its importance in the clock machinery.
621 Finally, our model integrates both mRNA and protein circadian datasets in a quantitative manner,
622 meaning that it does not only predict the phase and relative amplitude of the gene expression data as
623 existing models do [23, 65], but also the mean level, such information being critical for the connection
624 to PK-PD models. A very interesting perspective for future studies would be to consider coupling the
625 model by Woller *et al.* with ours to investigate the impact of feeding/fasting cycles on irinotecan
626 chronopharmacology.

627 Our core-clock model represents intracellular regulatory feedback loops that implicitly include extrinsic
628 circadian regulators such as temperature or light/dark cycles. Such external synchronizers were not
629 present in our cell culture setting, so that the SW480 and SW620 models are likely to represent the actual
630 events at stake. On the opposite, external or systemic regulators have a great influence on the mouse liver
631 clock. This precise question was the topic of another of our recent studies, in which we have explicitly
632 modelled the influence of temperature cycles and food intake on the core clock in four classes of mouse
633 (2 strains, 2 sexes) [66, 67]. Regarding CES2 modeling, we chose not to connect its protein degradation
634 rate directly to the core clock, since there is no published data regarding the existence or absence of such
635 molecular links. Thus, instead of including unreliable reactions to the model, we preferred to estimate
636 the circadian rhythm of CES2 protein degradation directly from the data. The parameter sensitivity
637 analysis evidenced the importance of this part of the model and strongly advocates the generation of
638 additional biological results about the circadian control of CES2 degradation.

639 Our experimental results obtained from time-dependent treatment using a CRC *in vitro* cellular system
640 highlight the cytotoxicity differences obtained by timing treatment, which were further emphasised by
641 our simulations. Compared to the predicted toxicity acrophase of the SW480 cell line, the toxicity
642 acrophase of the SW620 cell line is delayed by about four hours. In particular, the metastasis-derived
643 cell line showed the lowest variations in cytotoxicity among different treatment times. Our data also
644 shows a difference in terms of drug resistance between the two CRC cell lines, which, we hypothesize,
645 could be overcome if using treatment times of high cytotoxicity with the same amount of drug, or
646 potentially by increasing dosages in times of less toxicity. Yet, these are still speculative ideas, which
647 need further studies and validation in a clinical setting. The limited number of cell lines included in our
648 experimental setup present some limitations to the generalization of our findings and thus further
649 investigation of time-dependent treatment with a higher variety of cell lines and anticancer treatment
650 agents needs to be carried out in future research.

651

652 ***4.2 Personalized models to optimize timing in cancer treatment***

653 Chronotherapeutic studies aim at increasing treatment efficacy and minimizing toxicity for healthy cells
654 leading to a reduction of the side effects for patients [68]. Previous clinical results have shown that
655 personalization is a key element of successful chronotherapy outcome, for example, males and females
656 have shown different toxicities depending on treatment timing [6, 16, 69]. Sex should be considered as
657 a relevant determinant of circadian rhythms and optimal drug timing in the light of recent preclinical and
658 clinical findings [6, 16, 69]. Here, the mouse liver data was obtained from male mice, and the cell lines
659 were derived from a human male, so that the sex specificity seemed out of the scope of this study.
660 However, we have started to investigate the impact of sex on the circadian timing system as mentioned
661 above and did find significant sex-related differences in the shape and intensity of systemic controls on
662 the core clock, which augurs implications for drug optimal timing [66].

663

664 One aspect of personalized chronotherapy is an adaptation of medication timing to the patient's internal
665 time, which can be best assessed by a combination of mathematical modelling and machine learning [63].
666 Existing models of irinotecan PK-PD offer to predict best drug timing based on circadian rhythms of
667 proteins involved in irinotecan pharmacology, in the organ of interest (e.g. liver, or intestine) or in the
668 tumour. However, such datasets are unlikely to be obtained in the clinics on an individual patient basis
669 as it would involve multiple around-the-clock biopsies, which obviously raises questions of feasibility
670 and ethics regarding the benefit/risk ratio. Furthermore, circadian datasets on irinotecan-related proteins
671 would not be informative for personalizing the timing of other drugs, in particular the ones usually
672 combined with irinotecan (e.g. 5-fluorouracil, oxaliplatin). Instead, our new combined model provides
673 the option of computing irinotecan best timing from circadian rhythms of core-clock mRNA levels. The
674 major advantage of measuring core-clock genes – and not directly drug-related genes – is that it can be
675 done in any organ, since the peripheral core clock is synchronized across healthy tissues as suggested by
676 mouse and baboon studies [34]. Several patient-friendly methods for measuring clock-gene expression
677 in saliva or blood samples have been recently validated in the clinics (see [12] for a review). Furthermore,

678 strong oscillations, clearly above noise level, are expected in core-clock gene expression, which
679 facilitates the characterisation of their circadian profiles and reduces the number of needed time points
680 to do so [62]. In addition, a newly available statistical algorithm offers to derive clock gene mRNA
681 circadian rhythms from a single-time-point measurement of 10 clock genes [70]. Such methodology
682 could potentially be used to predict clock gene variations when only one time point is available, which
683 is often the case for the tumour. Our combined model could then be used to infer irinotecan personalized
684 best timing from clock-gene expression. As such chronoPK-PD models could be developed for any other
685 drug, optimal timing could be derived for multiple compounds from a single dataset of clock gene mRNA
686 circadian variations. In addition, instead of simplifying a patient's complex circadian profile to an
687 estimate of a value associated with their circadian time, by estimates based on a single time point
688 measurement, our model has the potential to fit the circadian rhythms of the patient based on their
689 personal gene expression data from peripheral tissues (e.g. saliva [62]), relevant to the clock-irinotecan
690 PK-PD network. Thus, in a clinical application, the model can be fitted both to the tumour clock and to
691 the healthy peripheral clock of the patient. Several therapeutic strategies may then be considered from
692 maximizing efficacy, or minimizing side effects, of a given drug dose, to more advanced approaches
693 aiming to optimize antitumor efficacy under strict tolerability constraints [26]. To exemplify the power
694 of our model for personalization, we fit the model to two different cell lines derived from human CRC
695 with cell line-specific toxicity profiles, which are different in the metastasis-derived cells as compared
696 to the primary tumour cells likely due to a disruption of the circadian profile and an alteration of
697 metabolism in the former cells [61]. Overall, our approach provides a promising direction for
698 mechanism-based chronotherapy personalization in the clinical setting.

699
700 The sensitivity analysis of the circadian toxicity profile is in accordance with the previously published
701 sensitivity analysis by Dulong *et al.* 2015 [27], highlighting especially the importance of CES2, which
702 is responsible for activation of irinotecan. Using our fitted mathematical model, changes in toxicity in
703 response to relevant alterations in core-clock or protein dynamics can in principle be predicted based on
704 circadian data for core-clock and drug-pharmacology genes. Further, the model can also be adapted for
705 patients with alterations in irinotecan PK-PD proteins, such as patients with increased sensitivity against
706 irinotecan due to a reduced UGT1A1 activity (reduced deactivation of SN-38) [71], or patients with a
707 decreased sensitivity to irinotecan due to an overexpression of ABC transporters, which leads to a faster
708 drug removal from the cell [72].

709 The strong influence of the core clock on the toxicity profile supports a strong dependence of optimal
710 treatment times on the personal circadian rhythm of patients, in accordance with previous reports [8]. In
711 particular, several core-clock parameters associated with *BMAL1* and *CLOCK* (*BMAL1* degradation rate,
712 *CLOCK* activation rate, cytosolic *BMAL1* degradation rate), show high sensitivity in our model,
713 highlighting the relevance of the core clock for irinotecan PK-PD. This is particularly relevant for cancer
714 patients, who often show alteration in their circadian rhythms that might be further changed during
715 hospitalization, as bedridden patients seem to have disrupted circadian rhythms [73-77]. This suggests
716 that even during a treatment frame of a few weeks, optimal treatment times might be shifted by a
717 flattening of the circadian rhythms. Light therapy might help to stabilize toxicity profiles, as it has been

718 shown to improve circadian oscillations in breast cancer patients [74]. Also melatonin administration or
719 pharmacological modulation of core-clock genes may have a positive impact on cancer therapy [78, 79].
720 We here report differently timed toxicity peaks for CRC cell lines. Naively, one would assume that cancer
721 cells show less robust oscillations compared to healthy cells, but this remains to be shown in future
722 research. While the toxicity of Caco-2 cells in the model of Dulong *et al.* was predicted following a
723 repeated 2-hour treatment [27], we here predict toxicity phase following a 84.5-h long treatment. The
724 situation in the patient is most likely somewhere between these values as irinotecan terminal half-life
725 after a 30-min infusion to colorectal cancer patients in the morning was approximately equal to 12h [68].
726 As the treatment administration scheme may present complex and chronomodulated shapes, irinotecan
727 whole-body pharmacokinetics must be precisely modelled in order to faithfully predict plasma and tissue
728 exposure concentrations.. A mathematical model relating infusion pump and administration schedules to
729 predict actual drug concentrations in the body has been developed [80], and a corresponding extension
730 could be used to further improve predictions of the here presented cellular model in a whole-body
731 context. Thus, for personalized medical treatments the personalization of mathematical models is key,
732 using easily accessible patient data to predict unassessable information relevant for medication.

733

734 *Conclusion*

735 Our clock-irinotecan model can be further optimized in a personalized manner and may be used to
736 predict the toxicity profile of a particular patient upon fitting his or her molecular circadian profile. The
737 model can be additionally used to investigate whether the differential regulation of PK-PD elements,
738 for example via additional medication with melatonin, can result in circadian toxicity profiles that
739 would support chronotherapy in irinotecan-treated cancers [78]. Altogether, our findings highlight the
740 relevance of investigating the effect of chronomodulated therapy in a clinical setting as it may
741 contribute to providing better personalized medical treatment with higher efficacy and lower
742 cytotoxicity, leading to a decrease of side effects and an increase of life quality for the patient.

743

744 ***Code availability***

745 The code can be downloaded from biomodels after publication of the manuscript.

746

747 ***Data availability***

748 The data that support the findings of this study are available from the corresponding author upon
749 reasonable request.

750 **Acknowledgments**

751 The work in A.R.'s group was supported by the German Federal Ministry of Education and Research
752 (BMBF)—eBio-CIRSPLICE – [FKZ031A316] and by the Dr. Rolf M. Schwiete Stiftung. O.A. was
753 additionally funded by the I4H program of the Charité - Universitätsmedizin Berlin. We acknowledge
754 support from the German Research Foundation (DFG) and the Open Access Publication Fund of the
755 Charité - Universitätsmedizin Berlin. The work in the group of A.B. was supported by INSERM, INRIA,
756 the ATIP-Avenir program, and the French Plan Cancer.

757

758 **Author contribution**

759 Conceived and designed the computational work: A.B., A.R.; Conceived and designed the experimental
760 work: A.R.; Performed the computational analysis: J.H., J.M.; Performed the experiments: O.A.;
761 Analysed the data: J.H., J.M., O.A., A.B., A.R.; Supervision: A.B., A.R. Wrote the original draft: J.H.,
762 J.M., A.R.; Critically read and contributed to write the paper: J.H., J.M., O.A., A.B., A.R.

763

764 **Competing Interests statement**

765 The authors declare that they have no competing interests.

766

767

768 **References**

769

- 770 1. Ko, C.H. and J.S. Takahashi, *Molecular components of the mammalian circadian clock*. Hum Mol Genet,
771 2006. **15 Spec No 2**(suppl_2): p. R271-7.
- 772 2. Matsuo, T., et al., *Control mechanism of the circadian clock for timing of cell division in vivo*. Science,
773 2003. **302**(5643): p. 255-9.
- 774 3. Bass, J. and J.S. Takahashi, *Circadian integration of metabolism and energetics*. Science, 2010.
775 **330**(6009): p. 1349-54.
- 776 4. Scheiermann, C., Y. Kunisaki, and P.S. Frenette, *Circadian control of the immune system*. Nat Rev
777 Immunol, 2013. **13**(3): p. 190-8.
- 778 5. Kim, D.W., E. Zavala, and J.K. Kim, *Wearable technology and systems modeling for personalized*
779 *chronotherapy*. Current Opinion in Systems Biology, 2020. **21**: p. 9-15.
- 780 6. Anderson, S.T. and G.A. FitzGerald, *Sexual dimorphism in body clocks*. Science, 2020. **369**(6508): p.
781 1164-1165.
- 782 7. El-Athman, R. and A. Religio, *Escaping Circadian Regulation: An Emerging Hallmark of Cancer?* Cell
783 Syst, 2018. **6**(3): p. 266-267.
- 784 8. Ballesta, A., et al., *Systems Chronotherapeutics*. Pharmacol Rev, 2017. **69**(2): p. 161-199.
- 785 9. Bollinger, T. and U. Schibler, *Circadian rhythms - from genes to physiology and disease*. Swiss Med
786 Wkly, 2014. **144**(2930): p. w13984.
- 787 10. Bicker, J., et al., *Timing in drug absorption and disposition: The past, present, and future of*
788 *chronopharmacokinetics*. Br J Pharmacol, 2020. **177**(10): p. 2215-2239.
- 789 11. Zhang, R., et al., *A circadian gene expression atlas in mammals: implications for biology and medicine*.
790 Proc Natl Acad Sci U S A, 2014. **111**(45): p. 16219-24.
- 791 12. Gaspar, L.S., et al., *The importance of determining circadian parameters in pharmacological studies*. Br J
792 Pharmacol, 2019. **176**(16): p. 2827-2847.
- 793 13. Innominato, P.F., et al., *Efficacy and safety of chronomodulated irinotecan, oxaliplatin, 5-fluorouracil*
794 *and leucovorin combination as first- or second-line treatment against metastatic colorectal cancer:*
795 *Results from the International EORTC 05011 Trial*. Int J Cancer, 2020. **n/a**(n/a).
- 796 14. Levi, F., et al., *Cetuximab and circadian chronomodulated chemotherapy as salvage treatment for*
797 *metastatic colorectal cancer (mCRC): safety, efficacy and improved secondary surgical resectability*.
798 Cancer Chemother Pharmacol, 2011. **67**(2): p. 339-48.
- 799 15. Giacchetti, S., et al., *Sex moderates circadian chemotherapy effects on survival of patients with*
800 *metastatic colorectal cancer: a meta-analysis*. Ann Oncol, 2012. **23**(12): p. 3110-3116.
- 801 16. Innominato, P.F., et al., *Sex-dependent least toxic timing of irinotecan combined with chronomodulated*
802 *chemotherapy for metastatic colorectal cancer: Randomized multicenter EORTC 05011 trial*. Cancer
803 Med, 2020. **9**(12): p. 4148-4159.
- 804 17. Religio, A., et al., *Ras-mediated deregulation of the circadian clock in cancer*. PLoS Genet, 2014. **10**(5):
805 p. e1004338.
- 806 18. Hesse, J., et al., *An Optimal Time for Treatment-Predicting Circadian Time by Machine Learning and*
807 *Mathematical Modelling*. Cancers (Basel), 2020. **12**(11): p. 3103.
- 808 19. Leloup, J.C. and A. Goldbeter, *Toward a detailed computational model for the mammalian circadian*
809 *clock*. Proc Natl Acad Sci U S A, 2003. **100**(12): p. 7051-6.
- 810 20. Forger, D.B. and C.S. Peskin, *A detailed predictive model of the mammalian circadian clock*. Proc Natl
811 Acad Sci U S A, 2003. **100**(25): p. 14806-11.
- 812 21. Becker-Weimann, S., et al., *Modeling feedback loops of the Mammalian circadian oscillator*. Biophys J,
813 2004. **87**(5): p. 3023-34.

- 814 22. Mirsky, H.P., et al., *A model of the cell-autonomous mammalian circadian clock*. Proc Natl Acad Sci U S
815 A, 2009. **106**(27): p. 11107-12.
- 816 23. Religio, A., et al., *Tuning the mammalian circadian clock: robust synergy of two loops*. PLoS Comput
817 Biol, 2011. **7**(12): p. e1002309.
- 818 24. Kim, J.K. and D.B. Forger, *A mechanism for robust circadian timekeeping via stoichiometric balance*.
819 Mol Syst Biol, 2012. **8**: p. 630.
- 820 25. Li, X.M., et al., *A circadian clock transcription model for the personalization of cancer chronotherapy*.
821 Cancer Res, 2013. **73**(24): p. 7176-88.
- 822 26. Ballesta, A., et al., *A combined experimental and mathematical approach for molecular-based
823 optimization of irinotecan circadian delivery*. PLoS Comput Biol, 2011. **7**(9): p. e1002143.
- 824 27. Dulong, S., et al., *Identification of Circadian Determinants of Cancer Chronotherapy through In Vitro
825 Chronopharmacology and Mathematical Modeling*. Mol Cancer Ther, 2015. **14**(9): p. 2154-64.
- 826 28. Mathijssen, R.H., et al., *Clinical pharmacokinetics and metabolism of irinotecan (CPT-11)*. Clin Cancer
827 Res, 2001. **7**(8): p. 2182-94.
- 828 29. de Man, F.M., et al., *Individualization of Irinotecan Treatment: A Review of Pharmacokinetics,
829 Pharmacodynamics, and Pharmacogenetics*. Clin Pharmacokinet, 2018. **57**(10): p. 1229-1254.
- 830 30. Fuhr, L., et al., *The Circadian Clock Regulates Metabolic Phenotype Rewiring Via HKDC1 and Modulates
831 Tumor Progression and Drug Response in Colorectal Cancer*. EBioMedicine, 2018. **33**: p. 105-121.
- 832 31. Narumi, R., et al., *Mass spectrometry-based absolute quantification reveals rhythmic variation of
833 mouse circadian clock proteins*. Proceedings of the National Academy of Sciences, 2016. **113**(24): p.
834 E3461-E3467.
- 835 32. Livak, K.J. and T.D. Schmittgen, *Analysis of relative gene expression data using real-time quantitative
836 PCR and the 2(-Delta Delta C(T)) Method*. Methods, 2001. **25**(4): p. 402-8.
- 837 33. El-Athman, R., L. Fuhr, and A. Religio, *A Systems-Level Analysis Reveals Circadian Regulation of Splicing
838 in Colorectal Cancer*. EBioMedicine, 2018. **33**: p. 68-81.
- 839 34. El-Athman, R., et al., *A Computational Analysis of Alternative Splicing across Mammalian Tissues
840 Reveals Circadian and Ultradian Rhythms in Splicing Events*. Int J Mol Sci, 2019. **20**(16).
- 841 35. Hansen, N. and A. Ostermeier, *Completely derandomized self-adaptation in evolution strategies*. Evol
842 Comput, 2001. **9**(2): p. 159-95.
- 843 36. Luck, S., et al., *Rhythmic degradation explains and unifies circadian transcriptome and proteome data*.
844 Cell Rep, 2014. **9**(2): p. 741-51.
- 845 37. Reppert, S.M. and D.R. Weaver, *Molecular analysis of mammalian circadian rhythms*. Annu Rev Physiol,
846 2001. **63**: p. 647-76.
- 847 38. Narumi, R., et al., *Mass spectrometry-based absolute quantification reveals rhythmic variation of
848 mouse circadian clock proteins*. Proc Natl Acad Sci U S A, 2016. **113**(24): p. E3461-7.
- 849 39. Yang, F., et al., *The molecular mechanism regulating the autonomous circadian expression of
850 Topoisomerase I in NIH3T3 cells*. Biochem Biophys Res Commun, 2009. **380**(1): p. 22-7.
- 851 40. Oishi, K., H. Shirai, and N. Ishida, *CLOCK is involved in the circadian transactivation of peroxisome-
852 proliferator-activated receptor alpha (PPARalpha) in mice*. Biochem J, 2005. **386**(Pt 3): p. 575-81.
- 853 41. Preitner, N., et al., *The orphan nuclear receptor REV-ERBalpha controls circadian transcription within
854 the positive limb of the mammalian circadian oscillator*. Cell, 2002. **110**(2): p. 251-60.
- 855 42. Zheng, X., et al., *RAE1 promotes BMAL1 shuttling and regulates degradation and activity of CLOCK:
856 BMAL1 heterodimer*. Cell Death Dis, 2019. **10**(2): p. 62.
- 857 43. Wang, J., et al., *Nuclear Proteomics Uncovers Diurnal Regulatory Landscapes in Mouse Liver*. Cell
858 Metab, 2017. **25**(1): p. 102-117.
- 859 44. Peters, R., *Nucleo-cytoplasmic flux and intracellular mobility in single hepatocytes measured by
860 fluorescence microphotolysis*. EMBO J, 1984. **3**(8): p. 1831-6.

- 861 45. Shimba, S., et al., *Deficient of a clock gene, brain and muscle Arnt-like protein-1 (BMAL1), induces*
862 *dyslipidemia and ectopic fat formation*. PLoS One, 2011. **6**(9): p. e25231.
- 863 46. Aryal, R.P., et al., *Macromolecular Assemblies of the Mammalian Circadian Clock*. Mol Cell, 2017. **67**(5):
864 p. 770-782 e6.
- 865 47. Schwanhausser, B., et al., *Global quantification of mammalian gene expression control*. Nature, 2011.
866 **473**(7347): p. 337-42.
- 867 48. Xu, G., et al., *Human carboxylesterase 2 is commonly expressed in tumor tissue and is correlated with*
868 *activation of irinotecan*. Clinical Cancer Research, 2002. **8**(8): p. 2605-2611.
- 869 49. Mathijssen, R.H., et al., *Irinotecan pathway genotype analysis to predict pharmacokinetics*. Clin Cancer
870 Res, 2003. **9**(9): p. 3246-53.
- 871 50. Pommier, Y., *Topoisomerase I inhibitors: camptothecins and beyond*. Nat Rev Cancer, 2006. **6**(10): p.
872 789-802.
- 873 51. Smith, N.F., W.D. Figg, and A. Sparreboom, *Pharmacogenetics of irinotecan metabolism and transport:*
874 *an update*. Toxicol In Vitro, 2006. **20**(2): p. 163-75.
- 875 52. Ciotti, M., et al., *Glucuronidation of 7-ethyl-10-hydroxycamptothecin (SN-38) by the human UDP-*
876 *glucuronosyltransferases encoded at the UGT1 locus*. Biochem Biophys Res Commun, 1999. **260**(1): p.
877 199-202.
- 878 53. Ueda, H.R., et al., *System-level identification of transcriptional circuits underlying mammalian circadian*
879 *clocks*. Nat Genet, 2005. **37**(2): p. 187-92.
- 880 54. Gascoyne, D.M., et al., *The basic leucine zipper transcription factor E4BP4 is essential for natural killer*
881 *cell development*. Nat Immunol, 2009. **10**(10): p. 1118-24.
- 882 55. Onishi, Y. and Y. Kawano, *Rhythmic binding of Topoisomerase I impacts on the transcription of Bmal1*
883 *and circadian period*. Nucleic Acids Res, 2012. **40**(19): p. 9482-92.
- 884 56. Zhao, M., et al., *E4bp4 regulates carboxylesterase 2 enzymes through repression of the nuclear receptor*
885 *Rev-erbalpha in mice*. Biochem Pharmacol, 2018. **152**: p. 293-301.
- 886 57. Ripperger, J.A., C. Jud, and U. Albrecht, *The daily rhythm of mice*. FEBS Lett, 2011. **585**(10): p. 1384-92.
- 887 58. Sancar, G. and M. Brunner, *Circadian clocks and energy metabolism*. Cell Mol Life Sci, 2014. **71**(14): p.
888 2667-80.
- 889 59. Sancar, A., et al., *Circadian clock control of the cellular response to DNA damage*. FEBS Lett, 2010.
890 **584**(12): p. 2618-25.
- 891 60. Gaucher, J., E. Montellier, and P. Sassone-Corsi, *Molecular Cogs: Interplay between Circadian Clock and*
892 *Cell Cycle*. Trends Cell Biol, 2018. **28**(5): p. 368-379.
- 893 61. Fuhr, L., et al., *The Circadian Clock Regulates Metabolic Phenotype Rewiring Via HKDC1 and Modulates*
894 *Tumor Progression and Drug Response in Colorectal Cancer*. EBioMedicine, 2018. **33**: p. 105-121.
- 895 62. Basti, A., et al., *Diurnal variations in the expression of core-clock genes correlate with resting muscle*
896 *properties and predict fluctuations in athletic performance across the day*. BMJ Open Sport & Exercise
897 Medicine, 2021. **in press**.
- 898 63. Hesse, J., et al., *An Optimal Time for Treatment-Predicting Circadian Time by Machine Learning and*
899 *Mathematical Modelling*. Cancers (Basel), 2020. **12**(11).
- 900 64. Furlan, A., et al., *Mathematical models converge on PGC1α as the key metabolic integrator of SIRT1 and*
901 *AMPK regulation of the circadian clock*. Proc Natl Acad Sci U S A, 2019. **116**(27): p. 13171-13172.
- 902 65. Woller, A., et al., *A Mathematical Model of the Liver Circadian Clock Linking Feeding and Fasting Cycles*
903 *to Clock Function*. Cell Rep, 2016. **17**(4): p. 1087-1097.
- 904 66. Martinelli, J., et al., *Model learning to identify systemic regulators of the peripheral circadian clock*.
905 2021.
- 906 67. Martinelli, J., et al., *Model learning to identify systemic regulators of the peripheral circadian clock*.
907 Bioinformatics, 2021. **37**(Suppl_1): p. i401-i409.

- 908 68. Levi, F., et al., *Circadian timing in cancer treatments*. *Annu Rev Pharmacol Toxicol*, 2010. **50**: p. 377-
909 421.
- 910 69. Li, X.M., et al., *A circadian clock transcription model for the personalization of cancer chronotherapy*.
911 *Cancer Res*, 2013.
- 912 70. Vlachou, D., et al., *TimeTeller: a New Tool for Precision Circadian Medicine and Cancer Prognosis*.
913 *bioRxiv*, 2019: p. 622050.
- 914 71. Fujii, H., et al., *Dose adjustment of irinotecan based on UGT1A1 polymorphisms in patients with*
915 *colorectal cancer*. *Cancer Chemother Pharmacol*, 2019. **83**(1): p. 123-129.
- 916 72. Fletcher, J.I., et al., *ABC transporters as mediators of drug resistance and contributors to cancer cell*
917 *biology*. *Drug Resist Updat*, 2016. **26**: p. 1-9.
- 918 73. Rida, P., M.I. Syed, and R. Aneja, *Time will tell: Circadian clock dysregulation in triple negative breast*
919 *cancer*. *Front Biosci (Schol Ed)*, 2019. **11**: p. 178-192.
- 920 74. Neikrug, A.B., et al., *Bright light therapy protects women from circadian rhythm desynchronization*
921 *during chemotherapy for breast cancer*. *Behav Sleep Med*, 2012. **10**(3): p. 202-16.
- 922 75. Ikegami, K., et al., *Interconnection between circadian clocks and thyroid function*. *Nat Rev Endocrinol*,
923 2019. **15**(10): p. 590-600.
- 924 76. Roenneberg, T. and M. Meroow, *The Circadian Clock and Human Health*. *Curr Biol*, 2016. **26**(10): p.
925 R432-43.
- 926 77. Innominato, P.F., et al., *The circadian timing system in clinical oncology*. *Ann Med*, 2014. **46**(4): p. 191-
927 207.
- 928 78. Gil-Martin, E., et al., *The emergence of melatonin in oncology: Focus on colorectal cancer*. *Med Res Rev*,
929 2019. **39**(6): p. 2239-2285.
- 930 79. Sulli, G., M.T.Y. Lam, and S. Panda, *Interplay between Circadian Clock and Cancer: New Frontiers for*
931 *Cancer Treatment*. *Trends Cancer*, 2019. **5**(8): p. 475-494.
- 932 80. Hill, R.J.W., et al., *Optimizing circadian drug infusion schedules towards personalized cancer*
933 *chronotherapy*. *PLoS Comput Biol*, 2020. **16**(1): p. e1007218.

934